Int J Fract
DOI 10.1007/s10704-007-9056-7

ORIGINAL PAPER

# Toughening due to domain switching in single crystal ferroelectric materials

**Jianshun Sheng · Chad M. Landis**

Received: 14 July 2006/ Accepted: 6 February 2007


**Abstract** In this paper Mode I steady state crack growth in single crystal ferroelectric materials is investigated. Specifically, the fracture toughness enhancement due to domain switching near a steadily growing crack tip is analyzed. For this purpose, an incremental phenomenological constitutive law for single crystal ferroelectric materials is implemented within a finite element model to calculate the stress and remanent strain fields around the crack tip. Also, the ratio of the far field applied energy release rate to the crack tip energy release rate, i.e. the toughening, is calculated. The numerical computations are carried out for single crystal ferroelectric materials of tetragonal or rhombohedral structure with different switching hardening and irreversible remanent strain levels. Toughening levels for crack growth along different crystallographic directions and planes are obtained and compared. Results from numerical computations for the toughening anisotropy for both tetragonal and rhombohedral crystals are presented and discussed.

J. Sheng · C. M. Landis
Department of Mechanical Engineering and Materials Science, MS 321, Rice University, P.O. Box 1892 Houston, TX 77251-1892, USA

C. M. Landis (✉)
Department of Aerospace Engineering and Engineering Mechanics, The University of Texas at Austin, 1 University Station, C0600, Austin, TX 78712-0235, USA
e-mail: landis@mail.utexas.edu

**Keywords** Fracture toughening · Ferroelectrics · Single crystal · Domain switching · Finite element methods

## 1 Introduction

Due to their unique electromechanical properties, ferroelectrics are useful materials for actuators and sensors. However, the fracture toughness of most ferroelectrics is only on the order of 1 MPa$\sqrt{\text{m}}$, and their inherent brittleness can limit their practical application. Therefore, it is worthwhile to investigate the fracture of ferroelectrics. A number of such investigations have already been carried out (Zhu and Yang 1997;Yang and Zhu 1998; Landis and McMeeking 1999; Kreher 2002; Landis 2002; Reece and Guiu 2002; Landis 2003, 2004a,b; Wang and Landis 2004, 2006). In contrast to the previous investigations, this paper will study fracture in single crystal ferroelectric materials under purely mechanical loading. Note that unpoled ferroelectrics remained unpoled under purely mechanical loading and exhibit purely ferroelastic response. The focus of the study is on the contribution of ferroelastic domain switching near the crack tip to the fracture toughness of the material. In this paper, a constitutive model similar to that in Huber et al. (1999) which assumes switching occurs at a critical driving force is developed for single crystal ferroelectric materials under purely

mechanical loading. It is cast in incremental form and captures characteristic features of ferroelastic behaviors of single crystal ferroelectric materials such as the asymmetry in the levels of attainable irreversible remanent strain in tension versus compression and the anisotropy associated with loading along different crystal axes. This constitutive law is implemented within finite element computations to determine the toughness enhancement due to switching near a crack tip in single crystal ferroelectric materials.

The remainder of the paper is organized as follows. Section 2 presents the constitutive law that is used to describe the ferroelastic behavior of single crystal ferroelectric materials. Section 3 presents the fracture model, crack growth criterion, and the finite element method into which the constitutive law is implemented to determine the stress and remanent strain fields around a steadily growing crack tip. Section 4 presents the simulation results for fracture toughness enhancement under various conditions. Finally, Sect. 5 will be used to conclude the paper.

## 2 The constitutive law for single crystal ferroelectrics

The non-linear constitutive behavior of single crystal ferroelectric materials results from domain switching due to the motion of domain walls within the crystal. A single crystal of ferroelectric material generally consists of many domains. Within a given domain, electrical polarization and dimensions of the unit cell all have an identical orientation. Domains are then separated by domain walls with adjacent domains each having a different crystallographic variant. Domain switching then occurs as domain walls move through the crystal, reducing the volume concentrations of certain variants in favor of the more energetically favorable variants. Such switching is responsible for the non-linear constitutive response of the ferroelectric single crystal. In this work tetragonal and rhombohedral crystal structures will be considered due to their technological importance. In a tetragonal crystal there are 6 possible polarization variants, and 8 polarization variants exists in a rhombohedral crystal. In this work, only the ferroelastic response of the material is of interest, and since any two variants with opposite polarization have identical spontaneous strain states, these two variant types can be counted together. Therefore, in a tetragonal crystal there are three possible strain variants of which the corresponding spontaneous strain tensors are

$$\begin{aligned}
\varepsilon_{ij}^{s,1} &= \varepsilon_0^{[100]}\left(\frac{3}{2}\delta_{1i}\delta_{1j} - \frac{1}{2}\delta_{ij}\right)\\
\varepsilon_{ij}^{s,2} &= \varepsilon_0^{[100]}\left(\frac{3}{2}\delta_{2i}\delta_{2j} - \frac{1}{2}\delta_{ij}\right)\\
\varepsilon_{ij}^{s,3} &= \varepsilon_0^{[100]}\left(\frac{3}{2}\delta_{3i}\delta_{3j} - \frac{1}{2}\delta_{ij}\right)
\end{aligned} \tag{2.1}$$

and in a rhombohedral crystal there are four possible variants of which the corresponding spontaneous strain tensors are

$$\begin{aligned}
\varepsilon_{ij}^{s,1} &= \frac{\varepsilon_0^{[111]}}{2}\left(\delta_{1i}\delta_{2j} + \delta_{2i}\delta_{1j} + \delta_{1i}\delta_{3j} + \delta_{3i}\delta_{1j}\right.\\
&\qquad \left.+\delta_{2i}\delta_{3j} + \delta_{3i}\delta_{2j}\right)\\
\varepsilon_{ij}^{s,2} &= \frac{\varepsilon_0^{[111]}}{2}\left(\delta_{1i}\delta_{2j} + \delta_{2i}\delta_{1j} - \delta_{1i}\delta_{3j} - \delta_{3i}\delta_{1j}\right.\\
&\qquad \left.-\delta_{2i}\delta_{3j} - \delta_{3i}\delta_{2j}\right)\\
\varepsilon_{ij}^{s,3} &= \frac{\varepsilon_0^{[111]}}{2}\left(-\delta_{1i}\delta_{2j} - \delta_{2i}\delta_{1j} - \delta_{1i}\delta_{3j} - \delta_{3i}\delta_{1j}\right.\\
&\qquad \left.+\delta_{2i}\delta_{3j} + \delta_{3i}\delta_{2j}\right)\\
\varepsilon_{ij}^{s,4} &= \frac{\varepsilon_0^{[111]}}{2}\left(-\delta_{1i}\delta_{2j} - \delta_{2i}\delta_{1j} + \delta_{1i}\delta_{3j} + \delta_{3i}\delta_{1j}\right.\\
&\qquad \left.-\delta_{2i}\delta_{3j} - \delta_{3i}\delta_{2j}\right)
\end{aligned} \tag{2.2}$$

Therefore, for the purposes of ferroelastic calculations, only 90° switching is considered in a tetragonal crystal, and 70° and 109° switching is considered in a rhombohedral crystal. In this work, the initial state of the ferroelectric crystal is that of a thermally depoled sample such that all possible crystallographic variants are equally likely, and the initial irreversible remanent strain is zero. As mechanical loading is applied eventually domain switching will occur causing an evolution of the volume fractions of the crystallographic variants. For a general state of variant volume concentrations, the remanent strain of the crystal, $\varepsilon_{ij}^r$, is given as

$$\varepsilon_{ij}^r = \sum_I \varepsilon_{ij}^{s,I} c^I \tag{2.3}$$

Given that we are most interested in the effects of domain switching and remanent straining on the

fracture toughness, we will neglect any differences in the orientation of the elastic properties of the variants. This simplification implies that the elastic properties of the crystal are assumed to be isotropic such that the total strain in the crystal is given by

$$\varepsilon_{ij} = \frac{1+\nu}{E}\sigma_{ij} - \frac{\nu}{E}\sigma_{kk}\delta_{ij} + \varepsilon^r_{ij} \tag{2.4}$$

where $\nu$ is the Poisson's ratio and $E$ is the Young's modulus. Given these assumptions, the rate of dissipation in the crystal can be shown to be

$$\dot{w}_D = \sigma_{ij}\dot{\varepsilon}^r_{ij} = \sum_I \sigma_{ij}\varepsilon^{s,I}_{ij}\dot{c}^I \tag{2.5}$$

We recognize that switching can occur along specific transformation systems, and we enumerate these systems such that switching from variant $I$ to variant $J$ is distinct from switching from $J$ to $I$ such that there are a total of 6 possible transformation systems for tetragonal crystals and 12 possible for rhombohedral crystals. Then defining $\dot{f}^\alpha$ to be the incremental volume of material transformed along transformation system $\alpha$, the incremental changes of variant volume concentrations are given as

$$\dot{c}^I = \sum_\alpha A^{I\alpha}\dot{f}^\alpha \tag{2.6}$$

Note that by definition the $\dot{f}^\alpha$ are always greater than or equal to zero. $A^{I\alpha}$ is the switching connectivity matrix, where $A^{I\alpha} = 1$ if the system $\alpha$ switches another variant into variant $I$, $A^{I\alpha} = -1$ if system $\alpha$ switches variant $I$ into another variant and $A^{I\alpha} = 0$ if system $\alpha$ is not associated with variant $I$. With this construction the dissipation rate can be written as

$$\begin{aligned}\dot{w}_D &= \sum_\alpha \sigma_{ij} \underbrace{\sum_I \varepsilon^{s,I}_{ij} A^{I\alpha}}\, \dot{f}^\alpha_{\Delta\varepsilon^\alpha_{ij}} = \sum_\alpha \underbrace{\sigma_{ij}\Delta\varepsilon^\alpha_{ij}}_{G^\alpha}\dot{f}^\alpha \\ &= \sum_\alpha G^\alpha \dot{f}^\alpha \end{aligned} \tag{2.7}$$

Here $G^\alpha$ can be identified as the energetic driving force on transformation system $\alpha$, and $\Delta\varepsilon^\alpha_{ij}$ is the spontaneous strain change associated with the system. Noting that by definition $\dot{f}^\alpha \geq 0$, and requiring that the dissipation rate be non-negative implies that switching can only occur if $G^\alpha > 0$. The specific form of the kinetic relationship between $G^\alpha$ and $\dot{f}^\alpha$ will assume that no transformation occurs up to a given limit on the driving force and rate dependent behavior occurs thereafter.

$$\dot{f}^\alpha = \dot{f}_0\left[\left(\frac{G^\alpha}{G^\alpha_c}\right)^{1/m} - 1\right] \quad \text{when} \quad G^\alpha \geq G^\alpha_c \tag{2.8}$$

and

$$\dot{f}^\alpha = 0 \quad \text{when} \quad G^\alpha < G^\alpha_c \tag{2.9}$$

Here $G^\alpha_c$ is the critical driving force for the activation of transformation system $\alpha$. The critical driving force $G^\alpha_c$ is assumed to be dependent upon the initial critical driving force $G^\alpha_0$ and the switching hardening $H_0$ as

$$G^\alpha_c = G^\alpha_0 + H_0\sum_I A^{I\alpha}c^I \tag{2.10}$$

in which the initial critical driving force $G^\alpha_0$ is defined as $G^\alpha_0 = G^{90^\circ}_c = 3\sigma^{[100]}_0\varepsilon^{[100]}_0/2$ for domain switching in a tetragonal crystal and $G^\alpha_0 = G^{70^\circ}_c = G^{109^\circ}_c = 4\sigma^{[111]}_0\varepsilon^{[111]}_0/3$ for domain switching in a rhombohedral crystal.

Within the finite element formulation the total strain at the time step $t + \Delta t$ is given and the previous state of the volume fractions of the variants are known. The purpose of the constitutive law outlined here is then to provide the updated levels of the variant volume fractions $c^{I,t+\Delta t}$. To accomplish this task, Eqs. 2.3–2.10 are integrated with a backward Euler method by solving the following equations governing the increments of the volume transformation rates $\Delta f^\alpha$ *on active systems only* at each time step,

$$\begin{aligned} h^\alpha\left(\Delta f^\beta\right) = &\left[G^\alpha_0 + H_0\sum_I A^{I\alpha}c^{I,t+\Delta t}\right]\left(\frac{\Delta f^\alpha}{\dot{f}_0\Delta t} + 1\right)^m \\ &- \Delta\varepsilon^\alpha_{ij}C_{ijkl}\left[\varepsilon^{t+\Delta t}_{kl} - \sum_I \varepsilon^{s,I}_{kl}c^{I,t+\Delta t}\right] = 0 \end{aligned} \tag{2.11}$$

where the $\Delta f^\beta$ are implicitly contained in $c^{I,t+\Delta t}$ and can be explicitly expressed as

$$c^{I,t+\Delta t} = c^{I,t} + \sum_\beta A^{I\beta}\Delta f^\beta \tag{2.12}$$

and the isotropic stiffness tensor $C_{ijkl}$ can be described in terms of $E$ and $\nu$ as

$$\begin{aligned} C_{ijkl} = &\frac{E}{2(1+\nu)}(\delta_{ij}\delta_{kl} + \delta_{il}\delta_{jk}) \\ &+ \frac{E\nu}{(1+\nu)(1-2\nu)}\delta_{ij}\delta_{kl} \end{aligned} \tag{2.13}$$

Equations (2.11) are solved by a Newton–Raphson technique, (2.12) is applied to update the volume concentrations, (2.3) is used to update the remanent strains, and $\sigma_{ij} = C_{ijkl}\left(\varepsilon_{kl} - \varepsilon^r_{kl}\right)$ is used to update the stresses. Given this updated stress state, the conditions that the assumed active systems in fact meet their transformation criteria are checked in order to ensure that a consistent set of active systems have been included in the solution.

In this paper, initially all possible crystallographic variants are equally likely, so the initial volume concentration of every variant is either

$$c_0^I = \frac{1}{3}, \quad I = 1, 2, 3 \tag{2.14}$$

for a tetragonal crystal or

$$c_0^I = \frac{1}{4}, \quad I = 1, 2, 3, 4 \tag{2.15}$$

for a rhombohedral crystal. Given these initial conditions and the strain history the solution for the evolution of the variant volume fractions can be marched through time. Thus the non-linear constitutive response of the ferroelectric single crystal is obtained, and it provides the evolution of the remanent strain history and the stress history given the total strain history. Figure 1 illustrates the stress versus strain hysteresis curves of a model single tetragonal crystal under cycling mechanical loading for different sets of the material parameters. All of these hysteresis curves are obtained through the computational simulation based on the constitutive model presented above. Notice the anisotropy in the tensile and compressive deformation. This non-linear constitutive law is implemented within the finite element model presented in the next section.

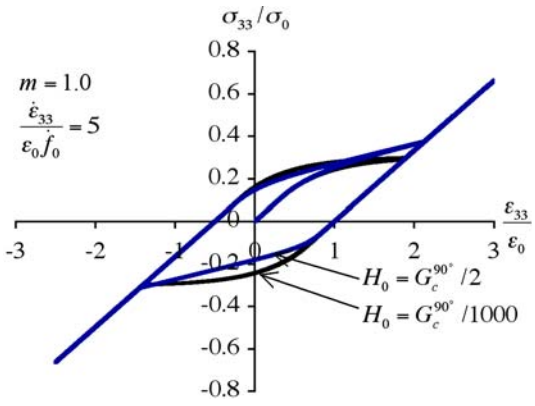


**Fig. 1** The stress–strain behavior for a tetragonal crystal loaded along a [100] direction at an intermediate strain rate for two distinct hardening levels. Note the anisotropy in the remanent strain levels that are achieved in tension versus compression

## 3 Fracture model and finite element implementation

In this paper small-scale switching analysis is performed on a steadily growing semi-infinite crack in a single ferroelectric crystal, and it is assumed that the characteristic height of the switching zone is much smaller than the crack length or any other specimen dimension. An asymptotic analysis is performed such that the remotely applied stresses can be characterized by the Mode I elastic K-field as

$$\begin{Bmatrix} \sigma_{11} \\ \sigma_{22} \\ \sigma_{12} \end{Bmatrix} = \frac{K_I}{\sqrt{2\pi r}} \cos\frac{\theta}{2} \begin{Bmatrix} 1 - \sin\frac{\theta}{2}\sin\frac{3\theta}{2} \\ 1 + \sin\frac{\theta}{2}\sin\frac{3\theta}{2} \\ \sin\frac{\theta}{2}\cos\frac{3\theta}{2} \end{Bmatrix} \quad \text{as} \quad r \to \infty \tag{3.1}$$

Here $K_I$ is the mode $I$ stress intensity factor, and $r$ and $\theta$ are the polar coordinates centered on the crack tip, with $\theta$ the angle between the radial direction and the $x$-axis, which is also the crack growth direction. Under plane strain conditions, the far field applied energy release rate $\mathcal{G}$ is related to the stress intensity factor $K_I$ by

$$\mathcal{G} = \frac{1 - \nu^2}{E} K_I^2 \tag{3.2}$$

The characteristic size of the switching zone under plane strain and small-scale switching conditions is given by its half height as

$$R_s = \frac{1}{3\pi}\left(\frac{K_I}{\sigma_0}\right)^2 = \frac{1}{3\pi}\frac{\mathcal{G}E}{(1-\nu^2)\sigma_0^2} \tag{3.3}$$

For the small scale switching assumption to be valid, this length must be small compared to the crack length.

A fracture criterion is required for the study of steady-state crack growth under small-scale switching conditions. Initially the crack tip is stationary. As the loading increases, a switching zone forms around the crack tip due to domain switching. As the loading continues to increase, the switching

zone will grow but the crack tip will remain stationary and will not propagate until the crack tip energy release rate, $\mathcal{G}_{\text{tip}}$, attains a material specific critical level of $\mathcal{G}_0$. So when $\mathcal{G}_{\text{tip}} = \mathcal{G}_0$, crack growth commences. This point corresponds to the crack growth initiation toughness on the *R*-curve for the material. As the crack growth continues, the far field applied loading must continue to increase in order to supply the dissipated energy in the domain switching wake due to the crack growth. Hence after crack initiation, the stress intensity factor $K_I$ and the far field applied energy release rate $\mathcal{G}$ must continue to increase, which corresponds to the rising portion of the *R*-curve. The crack continues to grow while $K_I$ and $\mathcal{G}$ continue to increase. After a significant amount of crack advance, steady growth conditions are met and the crack advances with $K_I$ and $\mathcal{G}$ at a constant level. This corresponds to the plateau on the toughness versus crack growth *R*-curve.

The focus of this paper is on the fracture toughness enhancement due to the domain switching around the steadily growing crack tip during the steady crack growth conditions. The toughening, or the fracture toughness enhancement, can be clearly shown by the ratio of the far field applied energy release rate during steady crack growth, denoted as $\mathcal{G}_{\text{ss}}$, to the crack tip energy release rate $\mathcal{G}_{\text{tip}}$. With the crack growth criterion presented above that the crack growth commences when $\mathcal{G}_{\text{tip}}$ reaches the intrinsic fracture toughness of the material $\mathcal{G}_0$, the ratio $\mathcal{G}_{\text{ss}}/\mathcal{G}_{\text{tip}}$, which then is also equal to $\mathcal{G}_{\text{ss}}/\mathcal{G}_0$, indicates the amount of the toughening due to the ferroelastic switching around the steadily growing crack tip, with $\mathcal{G}_{\text{ss}}/\mathcal{G}_{\text{tip}} = 1$ corresponding to absolutely no toughening.

In order to obtain the ratio $\mathcal{G}_{\text{ss}}/\mathcal{G}_{\text{tip}}$, $\mathcal{G}_{\text{ss}}$ and $\mathcal{G}_{\text{tip}}$ must be calculated first. The far field applied energy release rate during steady crack growth $\mathcal{G}_{\text{ss}}$ can be computed with Eq. 3.2 through $K_I$ which is related to the far field applied stress fields by Eq. 3.1. The crack tip energy release rate $\mathcal{G}_{\text{tip}}$ during steady crack growth can be determined with the following path-independent integral derived by Hutchinson (1974) for steady crack growth

$$\mathcal{G}_{\text{tip}} = I = \int_{\Gamma} (U n_x - \sigma_{ij} n_j u_{i,x}) \mathrm{d}\Gamma \tag{3.4}$$

where $\Gamma$ is a counterclockwise directed contour around the crack tip, $n_i$ are the components of the unit normal directed to the right along the contour, $u_i$ are the components of the displacement vector, and $U$ is the history dependent stress work density at a material point defined as

$$U = \int_0^{\varepsilon} \sigma_{ij} \, \mathrm{d}\varepsilon_{ij} \tag{3.5}$$

In the *I*-integral above, $\sigma_{ij}$ are the components of the stress tensor around the crack tip and Eq. 3.1 for the far field applied stress fields are not valid here due to the switching around this region. In order to calculate the mechanical fields near the crack tip, and hence $\mathcal{G}_{\text{tip}}$ with Hutchinson's *I*-integral and further the ratio $\mathcal{G}_{\text{ss}}/\mathcal{G}_{\text{tip}}$, a steady-state finite element procedure is implemented. This method was originally developed by Dean and Hutchinson [1980] and recently has been used by **?**Landis [2003b] to determine the toughening due to the ferroelastic switching in polycrystalline ferroelectrics. The finite element solution is used to compute the I-integral using the domain integral technique of Li et al. (1985). The formulation to derive the finite element method is based on the virtual work expression

$$\int_V \delta\varepsilon_{ij} C_{ijkl} \varepsilon_{kl} \, \mathrm{d}V = \int_S \delta u_i T_i \, \mathrm{d}S + \int_V \delta\varepsilon_{ij} C_{ijkl} \varepsilon^r_{kl} \mathrm{d}V \tag{3.6}$$

where $S$ is the boundary of the volume $V$, $C_{ijkl}$ are the Cartesian components of the isotropic stiffness tensor that can be written in terms of $E$ and $\nu$, specifically expressed in Eq. 2.13 for the single crystal ferroelectric material studies in this paper, and the tractions acting on the boundary $S$ are given as $T_i = \sigma_{ji} n_j$.

After the application of the appropriate finite element interpolations and the cancellation of the appropriate variational term, the left-hand side of Eq. 3.6 yields a linear elastic stiffness matrix dotted with a vector of unknown nodal displacements. Note that this stiffness matrix does not depend on any non-linear deformations, only on the finite element mesh geometry and elastic properties. The first term on the right-hand side is a vector of known applied nodal forces, and the second term is a residual body force vector due to the distribution of remanent strains in the material. In

order to solve finite element equations of Eq. 3.6, an iterative method is applied. Initially, the remanent strain is assumed to be zero at every point in the material. Therefore initially the body force due to the remanent strain is zero, and Eq. 3.6 is then solved and a new distribution of strains is obtained. Under steady-state crack growth conditions, all rates of the field quantities can be related to their derivatives to the coordinate in the crack growth direction $x$ through the crack growth rate $\dot{a}$ by $\dot{\phi} = -\dot{a}\frac{\partial \phi}{\partial x}$. Here $\phi$ is any scalar field quantity, for example a Cartesian component of stress or strain. Hence, in order to obtain the updated approximations to the stress and remanent strain distributions, the constitutive law described in Sect. 2 is integrated along streamlines of constant height above the crack plane from the right edge of the finite element mesh to the left with this new but approximate strain distribution. The new stress and remanent strain distributions are then applied in Eq. 3.6, which is solved for a new nodal displacement and further a new strain distribution. With the updated solution for the strains, the constitutive law is integrated along streamlines to yield an updated approximate distribution for the stress and remanent strain. This iterative procedure is continued until the solution for the nodal displacements, and hence the remainder of the mechanical fields, achieves a suitable level of convergence.

Within the finite element model for fracture of single crystal ferroelectric material, the stress and strain fields can be expressed in a normalized form as

$$\frac{\sigma_{ij}}{\sigma_0} = \bar{\sigma}_{ij}\left(\frac{x}{R_0}, \frac{y}{R_0}; \frac{\varepsilon_0 E}{\sigma_0}, \frac{H_0}{G_0^{\alpha}}, \nu\right) \tag{3.7}$$

$$\frac{\varepsilon_{ij}}{\varepsilon_0} = \bar{\varepsilon}_{ij}\left(\frac{x}{R_0}, \frac{y}{R_0}; \frac{\varepsilon_0 E}{\sigma_0}, \frac{H_0}{G_0^{\alpha}}, \nu\right) \tag{3.8}$$

where $\bar{\sigma}_{ij}$ and $\bar{\varepsilon}_{ij}$ represent dimensionless functions of the normalized spatial coordinates, the normalized material parameters and the other material properties. Here $R_0$ is the characteristic size of the switching zone given by Eq. 3.3 when $\mathcal{G} = \mathcal{G}_0$, explicitly expressed as

$$R_0 = \frac{1}{3\pi}\frac{\mathcal{G}_0 E}{(1-\nu^2)\sigma_0^2} \tag{3.9}$$

and is a material specific constant, $\varepsilon_0 E/\sigma_0$ is the ratio of irreversible remanent strain to the characteristic elastic strain in the material which is $\varepsilon_0^{[100]} E/\sigma_0^{[100]}$ for tetragonal crystals and $\varepsilon_0^{[111]} E/\sigma_0^{[111]}$ for rhombohedral crystals, and $H_0/G_0^{\alpha}$ is the normalized switching hardening. Finally, the switch toughening, the ratio of the steady state far field applied energy release rate $\mathcal{G}_{ss}$ to the crack tip energy release rate $\mathcal{G}_{tip}$, will depend on the dimensionless material parameters as

$$\frac{\mathcal{G}_{ss}}{\mathcal{G}_{tip}} = \frac{\mathcal{G}_{ss}}{\mathcal{G}_0} = \bar{\mathcal{G}}\left(\frac{\varepsilon_0 E}{\sigma_0}, \frac{H_0}{G_0^{\alpha}}, \nu\right) \tag{3.10}$$

Note that due to the rate dependence assumed in the material law, the fields and the toughening should also depend on the crack growth rate, the characteristic transformation rate $\dot{f}_0$, and the rate hardening exponent $m$. However, for the simulations to be presented, the crack growth rate has been chosen to be sufficiently slow such that the material exhibits essentially rate independent behavior and the fields and toughening are independent of these rate-type quantities. This point will be illustrated in the following section.

## 4 Results

### 4.1 Fracture toughness and crack growth rate

This work is concerned with modeling the rate independent toughness due to ferroelastic domain switching. However, the constitutive model being applied does contain rate dependence. Qualitatively, the following features are expected for the toughening. For sufficiently fast crack growth the material will not be allowed enough time to fully develop a switching zone and the behavior will essentially be elastic resulting in little to no toughening. At the other extreme, for very slow crack growth, the switching zone will be able to develop and fully relax at all points leading to a maximum level of dissipation and toughness enhancement. This work is concerned with the latter case and hence the concept of "very slow" crack growth needs to be quantified.

Simulations of crack growth in the [100] direction on a (010) crack plane at different crack growth rates were carried out for single crystal ferroelectric materials with tetragonal structure. The results for the toughening ratio as a function of the crack

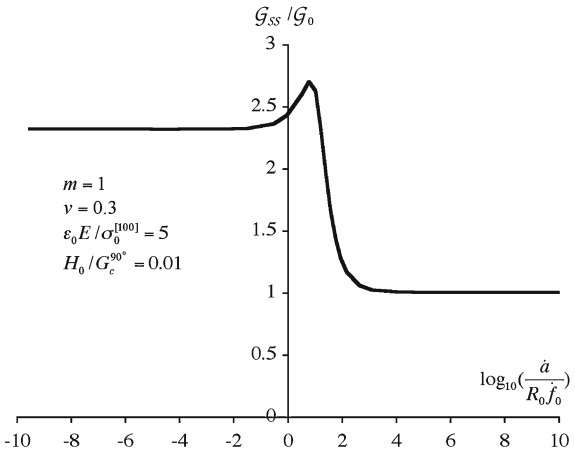


**Fig. 2** The level of toughness enhancement as a function of the crack growth rate. Simulations in this work are carried out at very slow crack growth rates in order to model rate independent behavior

growth rate for $m = 1$ are illustrated in Fig. 2. For crack growth rates above $10^4 R_0\dot{f}_0$ the toughness enhancement is negligible with the material responding in an essentially elastic manner. Note that even in these simulations there is domain switching and the size of the switching zone is approximately $R_0$. However, the intensity of the domain switching is exceedingly small such that the dissipation is negligible. At the other end of the spectrum, for normalized crack growth rates less than $10^{-1} R_0\dot{f}_0$ the switch toughening plateaus to a level of $2.3\mathcal{G}_0$ for the given set of material parameters. Hence, to model rate independent behavior, crack growth rates of $\dot{a} < 10^{-3} R_0\dot{f}_0$ have been used for the results to be presented in the following sections.

### 4.2 Fracture toughness versus the level of irreversible remanent strain

The primary goal of this paper is to determine how the steady-state fracture toughness enhancement in single crystal ferroelectric materials depends on the material properties and the direction and plane of crack growth. The most fundamental material parameter that has been identified in all switch and transformation toughening models is $\varepsilon_0 E/\sigma_0$, which explicitly is the ratio of spontaneous or transformation strain to the characteristic elastic strain in the material. Specifically, this ratio will be symbolized as $\varepsilon_0^{[100]} E/\sigma_0^{[100]}$ for tetragonal crystals and $\varepsilon_0^{[111]} E/\sigma_0^{[111]}$ for rhombohedral crystals. Detailed finite element simulations were performed for a range of spontaneous strain levels and two levels of hardening, for tetragonal crystals and rhombohedral crystals respectively.

Figure 3 plots $\mathcal{G}_{ss}/\mathcal{G}_0$ versus $\varepsilon_0^{[100]} E/\sigma_0^{[100]}$ for tetragonal crystals with crack growth along four different crystal directions. The four crack growth directions, corresponding to the four sets of toughness curves in Fig. 3, from the top (black) to the bottom (green), are crack growth in $[1\bar{1}0]$ on a (110) crack plane, crack growth in [100] on a (010) crack plane, crack growth in [101] on a (010) crack plane, and lastly crack growth in [100] on a $(01\bar{1})$ crack plane. For each crack growth system there are two toughness curves, one with hardening $H_0/G_0^\alpha = 0.001$ in Fig. 3a and the other with hardening $H_0/G_0^\alpha = 1$ in Fig. 3b. The first feature of note illustrated on these plots is that the fracture toughness enhancement increases monotonically with the spontaneous strain level. This indicates that a crystal with larger spontaneous strain can dissipate more energy and therefore possesses larger steady-state fracture toughness enhancement for a given crack system. A second interesting and intuitive behavior is that the fracture toughening is also dependent on the hardening during switching. For each of the crack systems, as the hardening increases, the fracture toughening deceases. Furthermore, this dependence is strongest in the $[1\bar{1}0](110)$ crack system and weakest in the $[100](01\bar{1})$ system. The final feature illustrated on these plots is the anisotropy of fracture toughness. As shown in Fig. 3, with identical spontaneous strain and hardening levels, crack growth on the $[1\bar{1}0](110)$ system shows the largest toughness enhancement due to switching, and crack growth on the $[100](01\bar{1})$ systems shows the smallest level of toughening. This anisotropy of the toughening is particularly obvious when the saturation level of irreversible strain is relatively large.

The sizes and shapes of the switching zones around steadily growing cracks in these four crack growth directions are also of interest, and can be used to explain the qualitative rankings of the

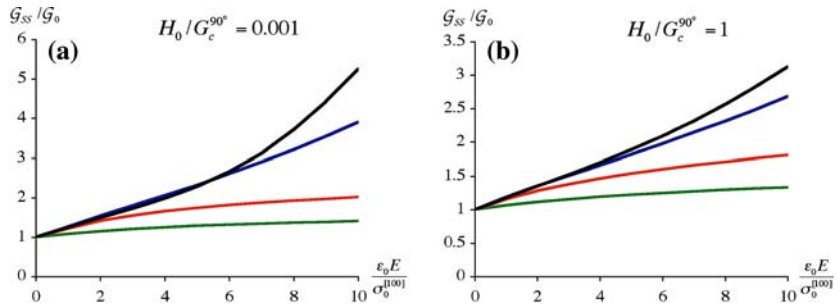


**Fig. 3** The toughening level versus the normalized spontaneous strain in a tetragonal material for steady crack growth in $[1\bar{1}0]$ on a (110) crack plane (black), crack growth in [100] on a (010) crack plane (blue), crack growth in [101] on a (010) crack plane (red), and lastly crack growth in [100] on a $(01\bar{1})$ crack plane (green). The two hardening levels are (**a**) $H_0/G_0^\alpha = 0.001$ and (**b**) $H_0/G_0^\alpha = 1$

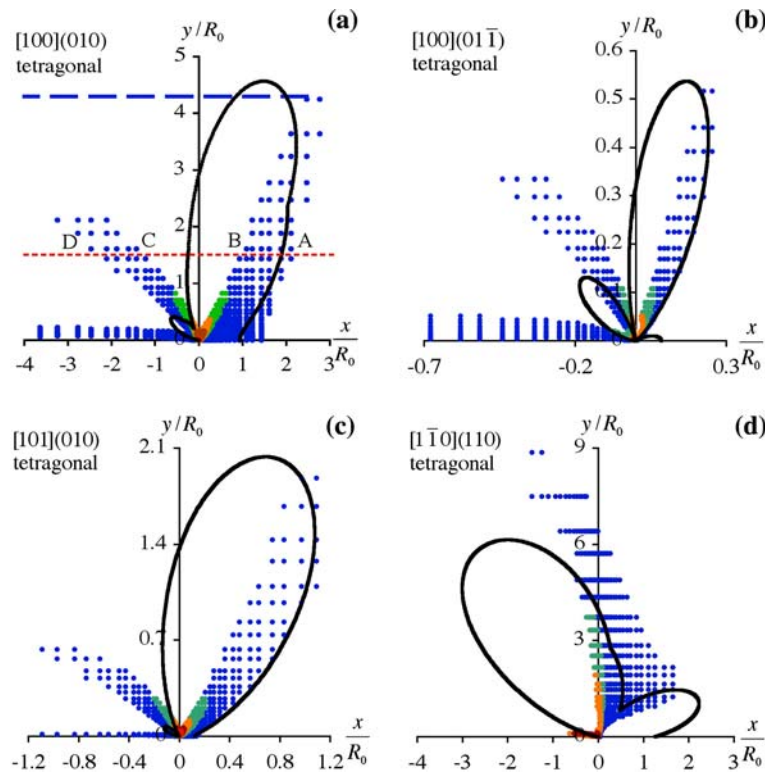


**Fig. 4** The active switching zones in tetragonal materials during steady crack growth on the (**a**) [100](010), (**b**) $[100](01\bar{1})$, (**c**) [101](010) and (**d**) $[1\bar{1}0](110)$ [crack growth direction]/(crack plane) systems. The colored dots are from the finite element simulations with $0 \le \bar{\varepsilon}^r \le 0.2$ blue, $0.2 \le \bar{\varepsilon}^r \le 0.4$ green, $0.4 \le \bar{\varepsilon}^r \le 0.6$ orange, $0.6 \le \bar{\varepsilon}^r \le 0.8$ brown, and $0.8 \le \bar{\varepsilon}^r \le 1$ red, with $\bar{\varepsilon}^r = \sqrt{2(\varepsilon_{ij}^r \varepsilon_{ij}^r/\varepsilon_0^2)/3}$ as the effective remanent strain, while the black lines are the zeroeth order approximation from the basic switching criteria of Eq. 2.8 and the asymptotic fields of Eq. 3.1

toughness enhancement due to switching. Fig. 4a–d shows the switching zones around a steadily growing crack in each of the four crack growth directions. The solid lines represent the small scale switching approximation to the initial switching zone shape, which are calculated by determining the boundary where the asymptotic stress field of Eq. 3.1 satisfies any of the transformation criteria. The dots are the finite element simulation results for the switching zone around a steadily growing crack. Due to the symmetry about the $x$-axis, the finite element computation only simulates the upper half plane, so only the upper half of the switching zone is shown in Fig. 4. As illustrated in Fig. 4, the switching zone around the crack growing steadily in the $[1\bar{1}0]$ direction on a (110) crack plane is the largest and also had the greatest fracture toughening of the four cases considered.

Furthermore, the switching zone around the crack growing in the [100] direction on a $(01\bar{1})$ crack plane is the smallest and also exhibits the lowest level of switch toughening of the four cases considered. Hence, there is a correlation between the volume of switched material near the crack tip and the level of toughening. However, we note that the volume of switched material is *in*dependent of the spontaneous strain level and additionally the intensity of switching at the outer boundary of the switching zone is minute, so this result must be interpreted accordingly. Ultimately, the intensity of the domain switching, which is highest very close to the crack tip, plays the most significant role in the level of toughness enhancement.

To understand the characteristics of the switching zone during steady crack growth, it is useful to consider the deformation processes that a material point experiences as the crack passes. For a coordinate system moving along with the crack, the dashed red line on Fig. 4a illustrates a specific streamline for a material point. A given material point begins at $x \to \infty$ and moves along the streamline in the negative $x$-direction. Prior to entering the active switching zone at point A, the stress state for the material point does not satisfy the transformation criteria for any of the switching systems and the material point responds elastically. At point A the transformation criterion for at least one switching system is satisfied and domain switching commences. Between points A and B, transformation is active and remanent strain accumulates at the material point. Upon exiting the active switching zone at point B the transformation criteria for all of the switching systems are no longer satisfied and domain switching stops. Between points B and C no additional switching occurs, but the variant volume concentrations and the accumulated remanent strains remain at the same state as at point B. As the material point reaches point C the transformation criterion for at least one of the switching systems is satisfied, and once again domain switching commences and changes to the variant volume concentrations and the remanent strain state occur. Domain switching continues to occur until the material point reaches D, where it exits the second lobe of active switching. From D to $x \to -\infty$ the material point responds elastically but with a residual remanent strain state equivalent to that at point D. This region behind the active switching zone is referred to as the wake of transformed/remanently deformed material. The blue dashed line on Fig. 4a denotes the full height of the transformed wake. Note, that each of the switching zone figures contains a similar wake, but the line is not drawn in order to reduce the clutter on these figures. The zones in these figures are regions of *active* transformation where the variant volume concentrations are changing. It is worth mentioning that prior theories assume that domain switching can occur only once as the crack tip passes. In the present calculations, it is the constitutive model that determines whether or not switching can occur, and the history of previous transformation does not preclude the possibility of reverse or additional switching at a point farther along the streamline. It is interesting to note that the secondary active switching lobes are similar in direction to those for the stationary case, but usually significantly larger in extent.

Figures 5a, b plot the toughness enhancement versus the spontaneous strain level for rhombohedral crystals. As for tetragonal crystals, rhombohedral crystals also exhibit increased toughening as the spontaneous strain increases, and the toughening decreases as the hardening increases. The primary difference between the rhombohedral and tetragonal crystals is the anisotropy of switch toughening. In rhombohedral crystals, it is in the [100] crack growth direction on $(01\bar{1})$ crack planes that the fracture toughness attains the largest value and shows the strongest dependence on saturation strain and switch hardening. The $[1\bar{1}0]$ crack growth direction on (110) crack planes exhibits the smallest toughening level and shows the weakest dependence on saturation strain and switching hardening.

The switching zones around steadily growing cracks for the four crack growth directions in rhombohedral crystals are illustrated in Fig. 6. As in Fig. 4, the black lines represent the approximation of the switching zone shape based on the stresses from Eq. 3.1 and the transformation criteria of Eq. 2.8, and the dots are the finite element simulation results. Again, there is a correlation between the switching zone size and the level of toughness enhancement. The switching zone around the steadily growing crack in the [100] direction with

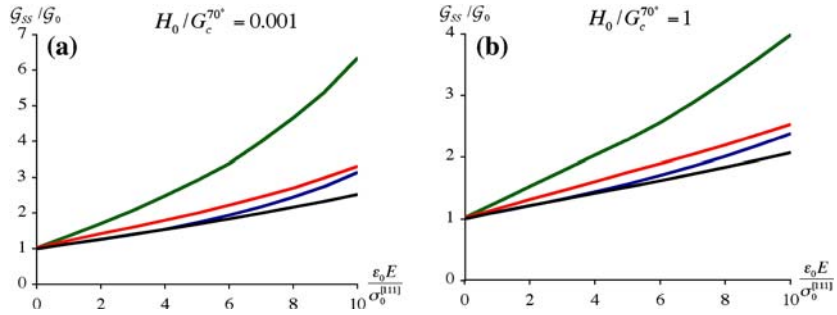


**Fig. 5** The toughening level versus the normalized spontaneous strain in a rhombohedral material for steady crack growth in [100] on a $(01\bar{1})$ crack plane (green), crack growth in [101] on a (010) crack plane (red), crack growth in [100] on a (010) crack plane (blue), and lastly crack growth in $[1\bar{1}0]$ on a (110) crack plane (black). The two hardening levels are (**a**) $H_0/G_0^{\alpha} = 0.001$ and (**b**) $H_0/G_0^{\alpha} = 1$

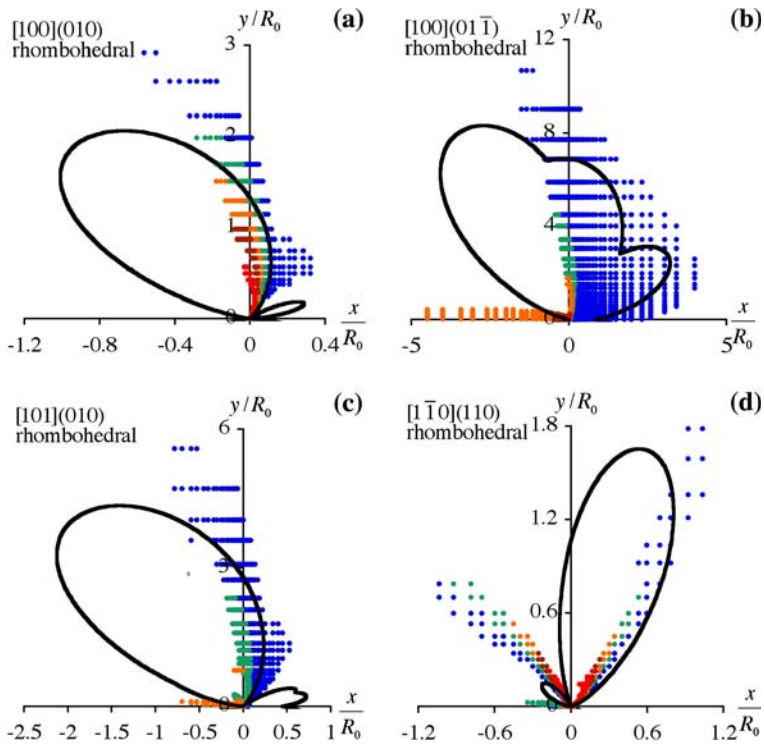


**Fig. 6** The active switching zones in rhombohedral materials during steady crack growth on the (**a**) [100](010), (**b**) [100](01$\bar{1}$), (**c**) [10$\bar{1}$](010) and (**d**) [1$\bar{1}$0](110) [crack growth direction]/(crack plane) systems. The colored dots are from the finite element simulations with $0 \le \bar{\varepsilon}^r \le 0.2$ blue, $0.2 \le \bar{\varepsilon}^r \le 0.4$ green, $0.4 \le \bar{\varepsilon}^r \le 0.6$ orange, $0.6 \le \bar{\varepsilon}^r \le 0.8$ brown, and $0.8 \le \bar{\varepsilon}^r \le 1$ red, with $\bar{\varepsilon}^r = \sqrt{2(\varepsilon_{ij}^r \varepsilon_{ij}^r/\varepsilon_0^2)/3}$ as the effective remanent strain

crack plane $(01\bar{1})$ is the largest, and the switching zone around the steadily growing crack in the $[1\bar{1}0]$ direction with crack plane (110) is the smallest.

### 4.3 Anisotropy of toughening—rotations about [100] directions

The fracture toughness enhancements due to domain switching for four crack growth directions are presented in the results above. It was shown that there is an anisotropy in the toughening and switching zone shapes and sizes for both tetragonal crystals and rhombohedral crystals. A more detailed investigation is developed here on the anisotropy of the toughening, and the relationship between the toughening and the crack growth direction—crack plane system for both tetragonal crystals and rhombohedral crystals is discussed.

Consider the crystal with its ⟨100⟩ directions initially aligned with the Cartesian axes. In this section

as depicted in Fig. 7a–c, three different rotations of the crystal will be considered, (a) a rotation through an angle $\theta_x$ about the $x$-axis such that the angles between the [010] and [001] directions and the $y$ and $z$ axes are $\theta_x$, (b) a rotation through an angle $\theta_y$ about the $y$-axis such that the angles between the [100] and [001] directions and the $x$ and $z$ axes are $\theta_y$, and (c) a rotation through an angle $\theta_z$ about the $z$-axis such that the angles between the [100] and [010] directions and the $x$ and $y$ axes are $\theta_z$. Each of these three cases are analyzed over the full range of angle for both tetragonal and rhombohedral crystals. Note the all of the simulations in case (a) have a crack growth direction of [100], and all of the simulations for case (b) have a crack plane normal to [010].

Figure 8 plots the levels of switch toughening versus each of the three rotation angles for (a) tetragonal and (b) rhombohedral crystals. It is clear that there is a significant qualitative difference in the anisotropy of the toughening for tetragonal versus rhombohedral crystals. For example, the $[1\bar{1}0](110)$ crack system exhibits the highest toughening level for tetragonal crystals but the lowest for the rhombohedral material. Conversely, the $[100](01\bar{1})$ crack system exhibits the highest toughening level for rhombohedral crystals but the lowest for the tetragonal crystals. For tetragonal crystals, when the crack growth is kept in the [100] direction, the fracture toughening is the largest when the crack plane is (010) or (001), referred to as $\theta_x = 0°$ and $\theta_x = 90°$, and is the smallest on a $(01\bar{1})$ crack plane, i.e. $\theta_x = 45°$. This situation is reversed for the rhombohedral crystal with growth in the [100] direction. For tetragonal crystals with a (010) crack plane, the fracture toughening is the largest with the crack growth in [100] or [001] directions, i.e. $\theta_y = 0°$ and $\theta_y = 90°$, and

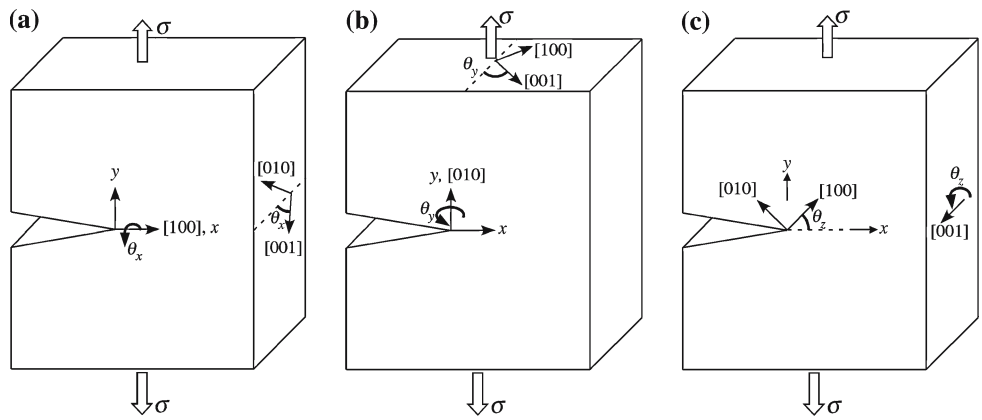


**Fig. 7** Schematics of the crystal orientation with respect to the crack growth direction and plane. (**a**) The definition of $\theta_x$. (**b**) The definition of $\theta_y$. (**c**) The definition of $\theta_z$

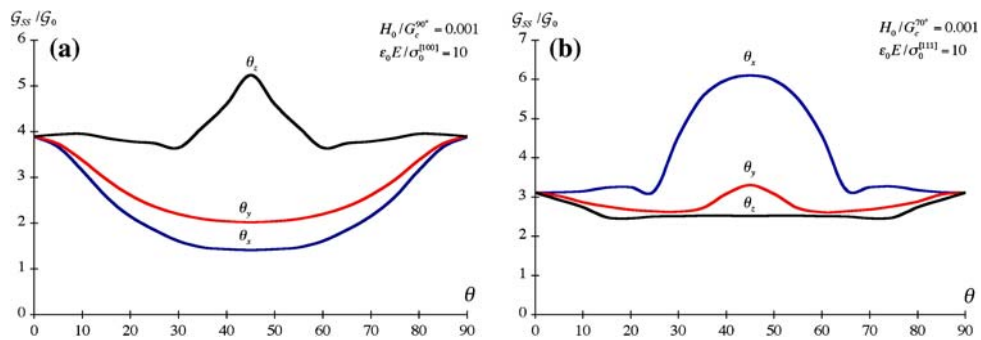


**Fig. 8** The toughness enhancement versus the three rotations of the crystal about the ⟨100⟩ directions for (**a**) tetragonal crystals and (**b**) rhombohedral crystals

is the smallest with the crack growth in the [101] direction, $\theta_y = 45°$. For the rhombohedral crystal the [100](010), [001](010), and [101](010) systems each exhibit similar toughening with the maximum on the [101](010) system, and the minima occur on the $[\sqrt{3}01](010)$ and $[10\sqrt{3}](010)$ systems. Finally, when the crack front is kept parallel to [001], for tetragonal crystals the fracture toughness is the largest on the $[1\bar{1}0](110)$ system ($\theta_z = 45°$) and smallest on the $[\sqrt{3}\bar{1}0](1\sqrt{30})$ ($\theta_z = 30°$) and $[\bar{1}\sqrt{30}]$ $(\sqrt{3}10)$ ($\theta_z = 60°$) systems, while the rhombohedral crystals exhibit the maximum toughening on the [100](010) ($\theta_z = 0°$) and $[0\bar{1}0](100)$ ($\theta_z = 90°$) and minima at $\theta_z = 20°$ and $\theta_z = 70°$.

When interpreting these results it should be noted that these calculations are for the level of *toughening* due to domain switching, not the fracture *toughness*. The fracture toughness is equal to the fracture toughening ratio times the fracture initiation toughness $\mathcal{G}_0$. Since it should be expected that $\mathcal{G}_0$ will be different on different crack planes, the toughening ratio $\mathcal{G}_{ss}/\mathcal{G}_0$ does not provide the entire fracture toughness picture. Hence other potentially low toughness systems include the ⟨101⟩ {010} systems for tetragonal crystals and the ⟨100⟩ {010} systems for rhombohedral crystals.

Switching zones around steadily growing cracks in selected directions associated with Fig. 8 are illustrated in Figs. 9 and 10 for tetragonal crystals and rhombohedral crystals respectively. In both crystal structure classes, the size of switching zones is larger when the corresponding toughening is high, and smaller when the corresponding toughening is low. It is also worth noting that in both tetragonal and rhombohedral crystals, the switching zone around a crack growing steadily in the

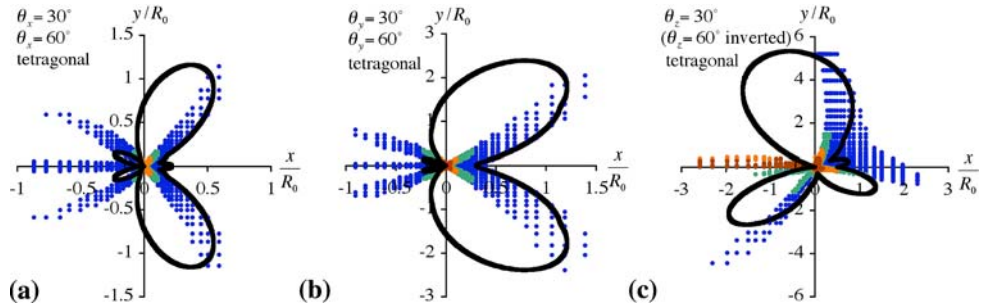


**Fig. 9** The active switching zones in tetragonal materials during steady crack growth on the (**a**) $[100](0\sqrt{3}\bar{1})$ or $[100](0\bar{1}\sqrt{3})$, (**b**) $[\sqrt{3}01](010)$ or $[10\sqrt{3}](010)$, and (**c**) $[\sqrt{3}\bar{1}0](1\sqrt{30})$ [crack growth direction]/(crack plane) systems. The colored dots are from the finite element simulations with $0 \le \bar{\varepsilon}^r \le 0.2$ blue, $0.2 \le \bar{\varepsilon}^r \le 0.4$ green, $0.4 \le \bar{\varepsilon}^r \le 0.6$ orange, $0.6 \le \bar{\varepsilon}^r \le 0.8$ brown, and $0.8 \le \bar{\varepsilon}^r \le 1$ red, with $\bar{\varepsilon}^r = \sqrt{2(\varepsilon^r_{ij}\varepsilon^r_{ij}/\varepsilon_0^2)/3}$ as the effective remanent strain

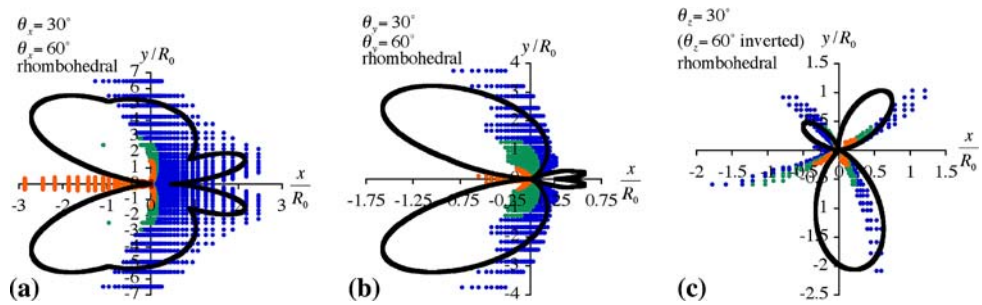


**Fig. 10** The active switching zones in rhombohedral materials during steady crack growth on the (**a**) $[100](0\sqrt{3}\bar{1})$ or $[100](0\bar{1}\sqrt{3})$, (**b**) $[\sqrt{3}01](010)$ or $[10\sqrt{3}](010)$, and (**c**) $[\sqrt{3}\bar{1}0](1\sqrt{30})$ [crack growth direction]/(crack plane) systems. The colored dots are from the finite element simulations with $0 \le \bar{\varepsilon}^r \le 0.2$ blue, $0.2 \le \bar{\varepsilon}^r \le 0.4$ green, $0.4 \le \bar{\varepsilon}^r \le 0.6$ orange, $0.6 \le \bar{\varepsilon}^r \le 0.8$ brown, and $0.8 \le \bar{\varepsilon}^r \le 1$ red, with $\bar{\varepsilon}^r = \sqrt{2(\varepsilon^r_{ij}\varepsilon^r_{ij}/\varepsilon_0^2)/3}$ as the effective remanent strain

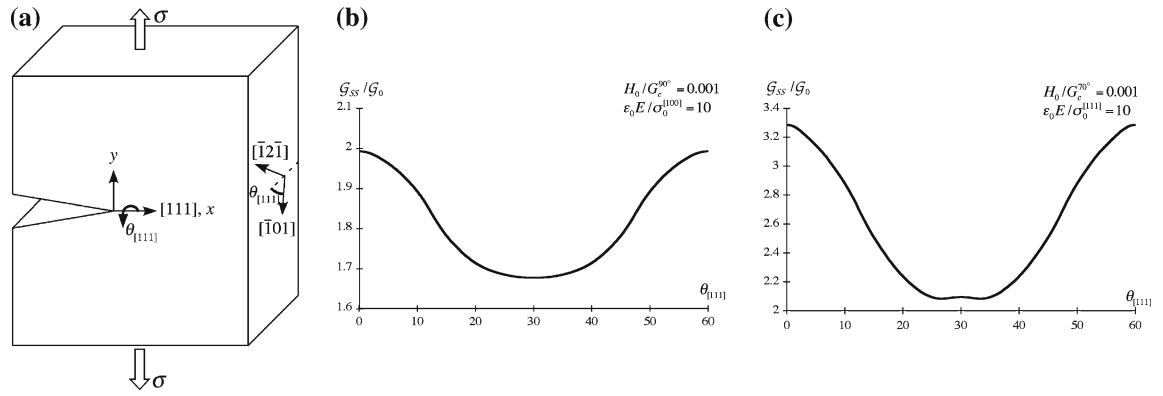


**Fig. 11** The toughness enhancement versus the rotation of the crystal about the [111] direction for crack growth in the [111] direction for (**b**) tetragonal crystals and (**c**) rhombohedral crystals. A schematic illustrating the definition of the angle $\theta_{[111]}$ is shown in (**a**)

[100] direction on a $(0\sqrt{3}\bar{1})$ crack plane ($\theta_x = 30°$) and the switching zone around a crack growing in the [100] direction on a $(0\bar{1}\sqrt{3})$ crack plane($\theta_x = 60°$) are identical and symmetric about the crack growth direction. This is also true for the switching zones around growing cracks for the $[\sqrt{3}01](010)$ case ($\theta_y = 30°$) and the $[10\sqrt{3}](010)$ case ($\theta_y = 60°$). In general, the switching zones for any set of $\theta_x$ and $90° - \theta_x$ or $\theta_y$ and $90° - \theta_y$ are the identical size and shape and symmetric about the crack growth direction. Lastly, the switching zone around a steadily growing crack in the $[\sqrt{3}\bar{1}0]$ direction on a $(1\sqrt{3}0)$crack plane ($\theta_z = 30°$) and the switching zone around crack steadily growing in the $[\bar{1}\sqrt{3}0]$ direction on a $(\sqrt{3}10)$ crack plane ($\theta_z = 60°$) have identical sizes and shapes but their positions are mirrored about the $x$-axis. In general, this is also true for any two switching zones for $\theta_z$ and $90° - \theta_z$, for both tetragonal crystals and rhombohedral crystals.

### 4.4 Toughening anisotropy with crack growth in the [111] direction

Crack growth in the [111] direction is also studied for both tetragonal crystals and rhombohedral crystals. Figure 11b plots the tetragonal crystal toughening curve with crack growth in [111] direction, and Fig. 11c plots the rhombohedral crystal toughening curve with crack growth in [111] direction. As the crystal coordinates rotate around [111], the crack plane normal also rotates, and when $\theta_{[111]} = 0°$, the crack plane is a $(\bar{1}2\bar{1})$ plane, as illustrated in Fig. 11.

Selected switching zones around steadily growing cracks in the [111] direction with different crack planes are illustrated in Fig. 12 for rhombohedral crystals. Note that the switching zone around a steadily growing crack in the [111] direction with a $(\bar{1}2\bar{1})$ crack plane ($\theta_{[111]} = 0°$) and the switching zone around crack steadily growing in the [111] direction with a $(\bar{2}11)$ crack plane ($\theta_{[111]} = 60°$) have identical size and shape but are mirrored about the $x$-axis. This mirroring of the switching zone is also true for any two switching zones with $\theta_{[111]}$ and $60° - \theta_{[111]}$. Only the switching zone for the crack with a $(\bar{1}10)$ crack plane ($\theta_{[111]} = 30°$) is symmetric about the $x$-axis for the [111] growth direction.

## 5 Summary

The toughening of single crystal ferroelectric materials under steady-state crack growth conditions has been investigated using an incremental constitutive law that models the nonlinear hysteretic stress–strain behavior due to domain switching. The constitutive law has been implemented within the finite element method to determine the mechanical fields around steadily growing cracks in the presence of ferroelastic domain switching. It has been shown that the amount of toughening due to domain switching is dependent on the level of spontaneous strain of the crystal variants, with

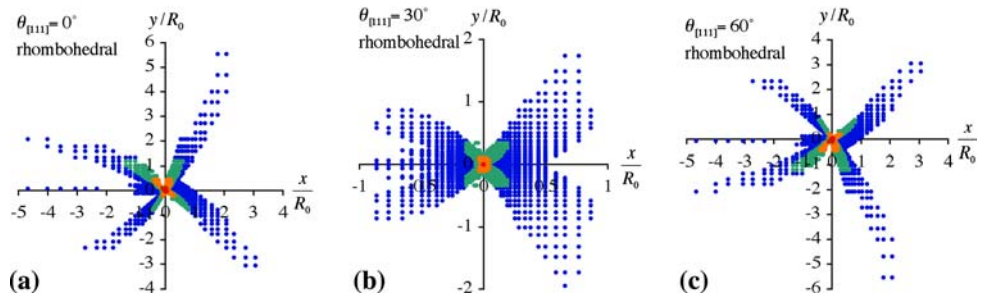


**Fig. 12** The active switching zones in rhombohedral crystals during steady crack growth on the (**a**) [111]($\bar{1}2\bar{1}$) (**b**) [111]($\bar{1}10$), and (**c**) [111]($\bar{2}11$) [crack growth direction]/(crack plane) systems. The colored dots are from the finite element simulations with $0 \le \bar{\varepsilon}^r \le 0.2$ blue, $0.2 \le \bar{\varepsilon}^r \le 0.4$ green, $0.4 \le \bar{\varepsilon}^r \le 0.6$ orange, $0.6 \le \bar{\varepsilon}^r \le 0.8$ brown, and $0.8 \le \bar{\varepsilon}^r \le 1$ red, with $\bar{\varepsilon}^r = \sqrt{2(\varepsilon^r_{ij}\varepsilon^r_{ij}/\varepsilon^2_0)/3}$ as the effective remanent strain

higher levels of spontaneous strain leading to more toughening. The toughening is also affected by amount of hardening that occurs during the progression of domain switching, with a decrease in toughening associated with the higher hardening materials. These qualitative descriptions of the behavior are true for both tetragonal and rhombohedral crystals.

The toughening anisotropy for both tetragonal and rhombohedral crystals has also been investigated with simulation results quantifying the toughening due to domain switching for cracks with different combinations of crack growth direction and crack plane. The differences in toughening anisotropy and the sizes and shapes of the domain switching zones for tetragonal crystals and rhombohedral crystals has also been illuminated. For tetragonal crystals, the largest toughening in the simulations is obtained when the crack steadily advances in the [$1\bar{1}0$] direction on a (110) crack plane, while in this case the toughening for rhombohedral crystals is quite small. For rhombohedral crystals, the largest toughening is obtained when the crack steadily grows in the [100] direction on a ($01\bar{1}$) crack plane, while in this case the toughening for tetragonal crystals is relatively small.

Finally, we note that the intrinsic fracture toughness $\mathcal{G}_0$ will be different on different crack planes, and hence the toughening ratio $\mathcal{G}_{ss}/\mathcal{G}_0$ does not provide the fracture toughness but rather the enhancement of the toughness due to domain switching. Depending on the intrinsic toughness of the different fracture planes, the potentially low toughness crack growth direction/plane systems that have been identified in this work include the $\langle 101\rangle\{010\}$, $\langle 100\rangle\{010\}$ and $\langle 111\rangle\{\bar{1}10\}$ systems for tetragonal crystals and the $\langle 101\rangle\{010\}$, $\langle 100\rangle\{010\}$, $\langle 1\bar{1}0\rangle\{110\}$ and $\langle 111\rangle\{\bar{1}10\}$ systems for rhombohedral crystals.

**Acknowledgements** The authors would like to acknowledge support from the Office of Naval Research grant number N00014-03-1-0537.

## References

Dean RH, Hutchinson JW (1980) Quasi-static steady crack growth in small scale yielding. In: Fracture mechanics, ASTM-STP 700, pp 383–405

Huber JE, Fleck NA, Landis CM, McMeeking RM (1999) A constitutive model for ferroelectric polycrystals. J Mech Phys Solids 47:1663–1697

Hutchinson JW (1974) On steady quasi-static crack growth. Harvard University Report, Division of Applied Sciences, DEAP S–8

Kreher WS (2002) Influence of domain switching zones on the fracture toughness of ferroelectrics. J Mech Phys Solids 50:1029–1050

Landis CM, McMeeking RM (1999) A phenomenological constitutive law for ferroelastic switching and a resulting asymptotic crack tip solution. J Intell Mater Systems Struct 10:155–163

Landis CM (2002) Uncoupled, asymmetric mode III and mode E crack tip solutions in non-linear ferroelectric materials. Eng Fract Mech 69:13–23

Landis CM (2003) On the fracture toughness of ferroelastic materials. J Mech Phys Solids 51:1347–1369

Landis CM (2004a) On the fracture toughness anisotropy of mechanically poled ferroelectric ceramics. Int J Fract 126:1–16

Landis CM (2004b) Energetically consistent boundary conditions for electromechanical fracture. Int J Solids Struct 41:6291–6315

Li FZ, Shih CF, Needleman A (1985) A comparison of methods for calculating energy release rates. Eng Fract Mech 21:405–421

Reece MJ, Guiu F (2002) Toughening produced by crack-tip-stress-induced domain reorientation in ferroelectric and/or ferroelastic materials. Philos Mag A 82:29–38

Wang J, Landis CM (2004) On the fracture toughness of ferroelectric ceramics with electric field applied parallel to the crack front. Acta Mater 52:3435–3446

Wang J, Landis CM (2006) Domain switch toughening in polycrystalline ferroelectrics. J Mater Res 21:13–20

Yang W, Zhu T (1998) Switching toughening of ferroelectrics subjected to electric fields. J Mech Phys Solids 46:291–311

Zhu T, Yang W (1997) Toughness variation of ferroelectrics by polarization switch under non-uniform electric field. Acta Mater 45:4659–4702